

See discussions, stats, and author profiles for this publication at: <https://www.researchgate.net/publication/295910965>

Enhancement of the Electrical Properties in BaTiO₃/PbZr_{0.52}Ti_{0.48}O₃ Ferroelectric Superlattices

Article in ACS Applied Materials & Interfaces · February 2016

DOI: 10.1021/acsami.5b12098

CITATIONS

0

READS

27

2 authors, including:



Bin He

Chinese Academy of Sciences, Shenyang, China

3 PUBLICATIONS 0 CITATIONS

SEE PROFILE

All content following this page was uploaded by [Bin He](#) on 26 April 2016.

The user has requested enhancement of the downloaded file. All in-text references [underlined in blue](#) are added to the original document and are linked to publications on ResearchGate, letting you access and read them immediately.

Enhancement of the Electrical Properties in BaTiO₃/PbZr_{0.52}Ti_{0.48}O₃ Ferroelectric Superlattices

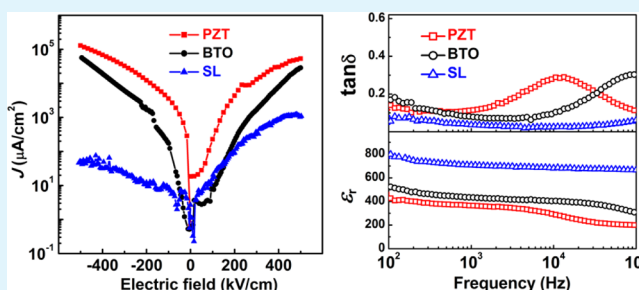
Bin He and Zhanjie Wang*

Shenyang National Laboratory for Materials Science, Institute of Metal Research (IMR), Chinese Academy of Sciences (CAS), 72 Wenhua Road, Shenyang 110016, China

S Supporting Information

ABSTRACT: In this study, BaTiO₃/Pb(Zr_{0.52}Ti_{0.48})O₃ (BTO/PZT) ferroelectric superlattices have been grown on the Nb-doped SrTiO₃ (NSTO) single-crystal substrate by pulsed laser deposition, and their electrical properties were investigated in detail. The leakage current was reduced significantly in the BTO/PZT superlattices, and the conduction mechanism could be interpreted as the bulk-limited mechanism. In addition, a more symmetric hysteresis loop was observed in the BTO/PZT superlattices compared with the pure PZT and BTO films. The BTO/PZT superlattices with the modulation thickness of 9.8 nm showed remarkably improved dielectric properties with dielectric constant and loss of 684 and 0.02, respectively, measured at the frequency of 10 kHz. Based on these experimental results, it can be considered that the BTO/PZT interfaces play a very important role for the enhanced electrical properties of the BTO/PZT superlattices.

KEYWORDS: ferroelectric superlattices, microstructure, leakage current, ferroelectric properties, dielectric properties

**INTRODUCTION**

Ferroelectric thin films have attracted much attention because of their technological applications in memory devices due to their excellent ferroelectric and dielectric properties.^{1–3} To realize high properties of the memory devices, for example, nonvolatile ferroelectric random access memories (NV-FRAM) and dynamic random access memory (DRAM), it is required to overcome the reliability problems in the ferroelectric thin films such as the high leakage, the notable imprint, and the high dielectric loss compared with the bulk counterparts.⁴

The performance of ferroelectric films is intimately entwined with the crystal structure and microstructures. In past decades, to improve electrical properties of the ferroelectric thin films such as reducing the leakage current and dielectric loss, modifying the imprint, and increasing dielectric constants, great efforts have been made, such as doping, developing new preparation method, and using different buffer layers and compositional gradation.^{5–7} Among various approaches, forming ferroelectric superlattices with well-organized interfaces would be a flexible and efficient method to manipulate the electrical properties.^{8–11} Lee et al. have fabricated a series of BaTiO₃-based superlattices and found an enhancement in the ferroelectric and dielectric properties with respect to pure BaTiO₃ films.¹² Generally, the improvement in the electrical properties of ferroelectric superlattices is mainly attributed to the strain effects, because of the different crystalline structures of parent materials or a large lattice mismatch between the parent materials.^{11–15} Recently, Okatan et al. reported that the electrostatic coupling at ordered interfaces can also play an

important role in determining the electrical properties of the ferroelectric superlattices.¹⁶ Some recent theoretical studies also suggested that the presence of space charges at the artificial interfaces can influence the strength of electrostatic coupling between the two ferroelectric layers.^{16–18} To understand the mechanism of the interface effects on the electrical properties in the ferroelectric superlattices, it is important to choose appropriate parent materials to avoid the strain effects.

In this study, we select the BaTiO₃ (BTO) and Pb(Zr_{0.52}Ti_{0.48})O₃ (PZT) as the constituent materials for the ferroelectric superlattices. One reason is that both PZT and BTO are the practical ferroelectric materials and have the same crystalline structure with a very similar lattice constant at room temperature. The lattice mismatching between them is very small (~1.0%), much less than that between the BaTiO₃ and SrTiO₃ in the BaTiO₃/SrTiO₃ superlattices (~2.3%).^{11,12,19} This allows us to prepare the high-quality ferroelectric superlattices with a minimum of structural defects in the interfaces. Another reason is that the values of spontaneous polarization are about 20 μC/cm² and over 60 μC/cm² for the (001)-oriented BTO and PZT films,^{12,20} respectively, so that there is a large polarization mismatch between them. Therefore, the BTO/PZT superlattices may be expected as an appropriate system to study the effect of polarization coupling. In this study, we focus on the fabrication of BTO/PZT superlattices and

Received: December 11, 2015

Accepted: February 25, 2016

Published: February 25, 2016

investigate their structural and electrical properties compared with the epitaxial BTO and PZT thin films.

EXPERIMENTAL SECTION

Nb-doped SrTiO₃ single-crystal plates (Nb:SrTiO₃ with 0.7 wt % of Nb, abbreviated as NSTO) with (100) orientation were used as substrates. Before depositing, the NSTO substrates were cleaned by alcohol and then acetone. The BTO/PZT superlattices were prepared by pulsed laser deposition on the (100)-oriented NSTO substrates, using a KrF excimer laser at a wavelength of 248 nm. Figure 1 shows

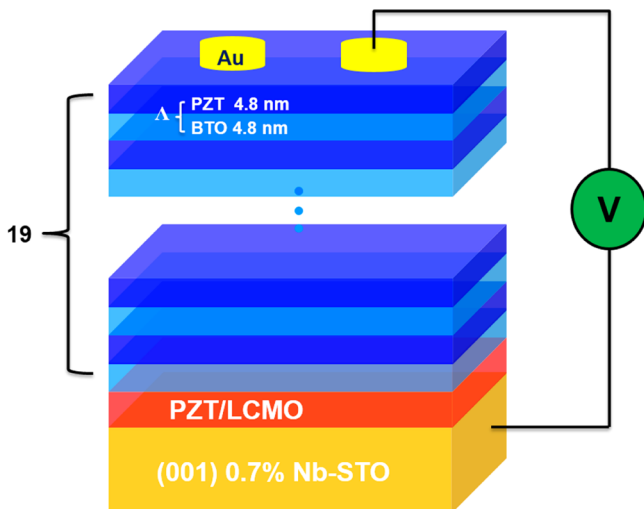


Figure 1. Schematic diagram of the (PZT_{4.8 nm}/BTO_{4.8 nm})₁₉ superlattices growing on the PZT/LCMO/(001) STO substrates.

the schematic diagram of the (BTO/PZT)₁₉ ferroelectric superlattices grown on the NSTO substrates. First, a La_{0.7}Ca_{0.3}MnO₃ (LCMO) epitaxial film with a thickness of 4 nm was deposited as a buffer layer to prevent polarization loss and leakage current for ferroelectric superlattices grown on the n-type Nb-doped SrTiO₃ substrates.²¹ Then, a 5 nm PZT layer was deposited on the top of the LCMO layer to reduce the lattice mismatching between the BTO and LCMO layers.¹⁴ Next, the BTO and PZT layers with the same thickness were grown at a temperature of 650 °C in oxygen atmosphere under 5 Pa, by alternating the BTO and PZT targets for 19 periods. For comparison, we also fabricated the pure PZT (~120 nm) and BTO (~200 nm) thin films on the LCMO-covered NSTO substrates under the same deposition parameters, respectively.

The crystal structure of the BTO/PZT superlattices was analyzed by X-ray diffraction (XRD; Rigaku, D/max-2000, Cu K α radiation, Tokyo, Japan). The surface morphology and roughness of the thin films was measured by atomic force microscope (AFM) in contact mode (Nanoscope IV, Digital Instruments, Tonawanda, NY, USA). The thickness and interface microstructure were observed by transmission electron microscopy (TEM; F20, Tecnai, Eindhoven, The Netherlands). Top Au electrodes with area of 0.1963 mm² were fabricated by sputtering. The electrical measurements were carried out using an Au-insulator-NSTO configuration, as shown in Figure 1. The polarization versus electric field (*P*-*E*) hysteresis loops and leakage current were measured at room temperature by using a standard ferroelectric test system (TF2000E; Aixacct, Aachen, Germany). The dielectric constants and dielectric losses were measured in a frequency range of 10²-10⁵ Hz at bias voltage of 100 mV using an impedance analyzer LCR Hitester (HIOKI 3532-50).

RESULTS AND DISCUSSION

Figure 2 shows XRD patterns of the BTO/PZT superlattices compared with the pure PZT and BTO films. For all samples, only (00*l*) diffraction peaks can be observed for both films and

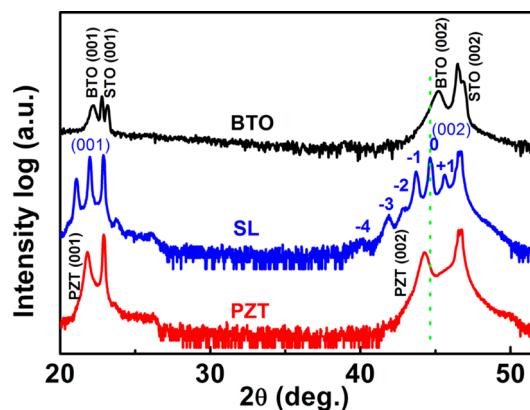


Figure 2. X-ray θ - 2θ diffraction patterns of pure PZT film, pure BTO film, and BTO/PZT superlattices.

substrates, suggesting that the PZT film, BTO film, and BTO/PZT superlattices are epitaxially grown on the NSTO substrates. The XRD pattern for the BTO/PZT superlattice shows the main peak (labeled as “0”) accompanied by characteristic satellite peaks (denoted as ± 1 , ± 2 , ...), which clearly indicate that the periodically modulated structure is achieved. The modulation period (Λ) in superlattices can be calculated from XRD patterns using the following relation:²²

$$\Lambda = \lambda_x / 2 (\sin \theta_{n+1} - \sin \theta_n) \quad (1)$$

where λ_x is the X-ray wavelength (0.15418 nm) and θ_{n+1} and θ_n are the angular positions of two adjacent satellite peaks. The modulation period (Λ) in the BTO/PZT superlattices calculated from the XRD patterns is to be about 101 Å. According to the position of the main peak, we can calculate the average out-of-plane lattice parameter (c_{av}) of the BTO/PZT superlattice to be 4.056 Å, which is between the values of the single films of PZT ($c_{PZT} \approx 4.097$ Å) and BTO ($c_{BTO} \approx 4.015$ Å). Moreover, the relationship between the out-of-plane lattice parameters of the BTO/PZT superlattice and the single films of PZT and BTO satisfies the following formula: $c_{av} \approx (c_{PZT} + c_{BTO})/2$. This can also be confirmed by the following TEM results. Therefore, it can be concluded that the strain in the BTO/PZT superlattices mainly derived from the constraints of the substrate, because of the good lattices matching between the PZT and BTO.

The surface morphologies the PZT and BTO films and the BTO/PZT superlattices were evaluated by AFM, and the results are shown in Figure 3. In all of the cases, the surface morphologies are very smooth without the formation of visible particles, and the root-mean-square roughness was determined to be lower than 0.4 nm. The microstructure of the BTO/PZT superlattices was further studied by TEM. Figure 4a shows a low-magnification TEM image of the BTO/PZT superlattices with the 19 modulation periods of BTO/PZT. The total thickness of the BTO/PZT superlattices is about 190 nm, and the individual thickness for the PZT and BTO layers is about 48 Å, respectively. So the thickness of one modulation period is about 96 Å, which is consistent with the XRD results. The high-resolution image (Figure 4b) shows that the BTO and PZT layers have grown epitaxially on each other with sharp interfaces. The epitaxial relationships between the BTO and PZT layers can be also confirmed by the fast Fourier transform (FFT) patterns transformed from the high-resolution TEM image of Figure 4b, as shown in Figure 4c. The epitaxial

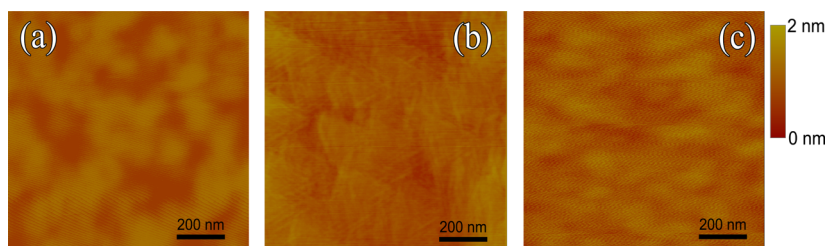


Figure 3. Surface morphologies of (a) the pure PZT film, (b) the pure BTO film, and (c) the BTO/PZT superlattices measured by AFM with contact mode. The scan size is $1 \times 1 \mu\text{m}^2$.

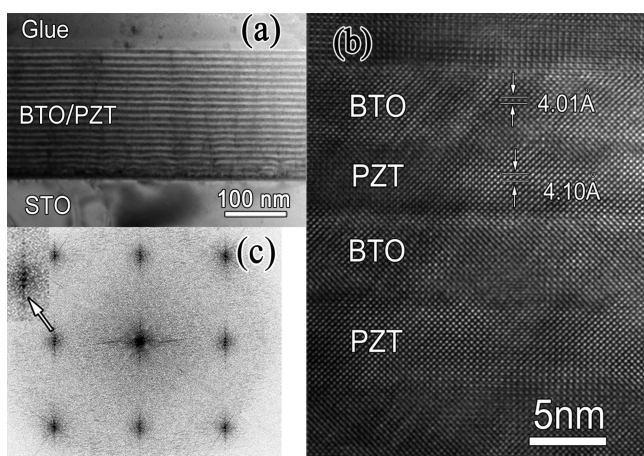


Figure 4. Low-resolution (a) and high-resolution (b) cross-sectional TEM image of BTO/PZT superlattices and (c) the fast Fourier transform (FFT) patterns of the HRTEM image of panel b.

relationship between the BTO and PZT layers is $(0\ 0\ 1)_{\text{BTO}}// (0\ 0\ 1)_{\text{PZT}}$ and $(0\ 1\ 0)_{\text{BTO}}// (0\ 1\ 0)_{\text{PZT}}$. The regular superlattice spots along the out-of-plane direction can be clearly observed in the inset in Figure 4c, which demonstrate that the BTO/PZT superlattices were grown by the growth mode of layer by layer with the well-defined periodicity.²³ Combined with the XRD results, we can conclude that high-quality ferroelectric superlattices have been prepared by using the constituents of PZT and BTO. The electrical properties of the BTO/PZT superlattices will be investigated in the following.

Figure 5a shows that the leakage current properties (J) as a function of electric field (E) of the BTO/PZT superlattices and the pure PZT and BTO films at room temperature. For the BTO/PZT superlattices, the leakage current density has been reduced by 2–3 orders of magnitude compared with both pure BTO and PZT films. A similar phenomenon has also been reported in the $\text{PbTiO}_3/\text{SrTiO}_3$ superlattices by Dawber et al.⁸ They pointed out that inserting the high resistance of a SrTiO_3 layer can decrease the leakage current of ferroelectric superlattices. However, it cannot explain our result, because the higher leakage current is observed in the BTO and PZT thin films. To further understand this phenomenon, we have measured the leakage current of the BTO/PZT superlattices with the different modulation periods and same total thickness (Supporting Information Figure S1). It has been shown that the leakage current of ferroelectric superlattices decrease with the decrease of the modulation periods, indicating that the leakage current of the BTO/PZT superlattices mainly attribute to their own, rather than the interfaces of ferroelectric/electrode. It has been well-accepted that the bulk limited conduction mechanisms in ferroelectric films include two kinds: the space-charge-

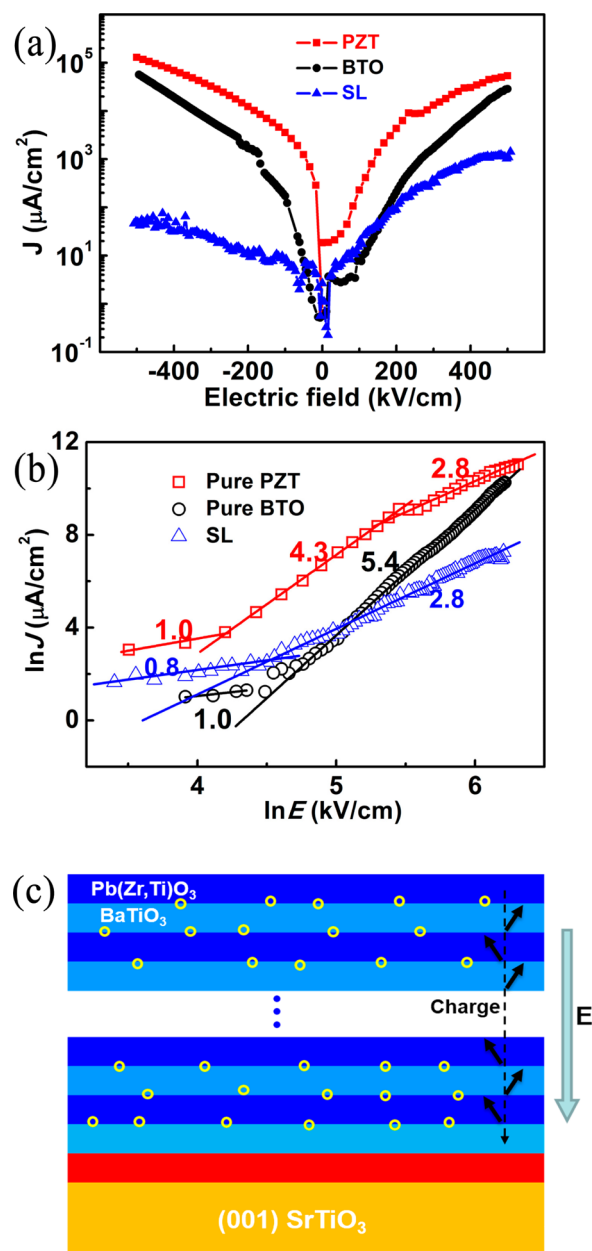


Figure 5. (a) Leakage current density (J) as a function of the electric voltage (E) for the pure PZT and BTO films and BTO/PZT superlattices. (b) $\ln J$ versus $\ln E$ for the pure PZT films, BTO films, and BTO/PZT superlattices at a positive bias (the values of the slope of the fitted lines are marked). (c) Schematic diagram to show the large space charges concentration accumulated to the interface and the movement of charges in an electric field. The yellow circles represent the space charges.

limited current (SCLC) and the Poole–Frenkel emission. The J – E curves of the BTO/PZT superlattices cannot be fitted well by the Poole–Frenkel emission mechanism, implying that this conduction mechanism is not suitable for the BTO/PZT superlattices. As can be seen from Figure 5b, the J – E curves at the positive bias for the BTO/PZT superlattices can be fitted quite well by the SCLC mechanism and described by Child's law:²⁴

$$J \propto \mu \epsilon_0 \epsilon_r E^\alpha / d \quad (2)$$

where μ is the charge carrier mobility, ϵ_0 is the permittivity of free space, ϵ_r is the relative dielectric constant, d is the film thickness, and α is a trap-dependent exponential factor. At high electric fields, α is about 2.8, which means trap-controlled SCLC. And the leakage current of BTO/PZT superlattices at different temperatures can also be fitted well with trap-controlled SCLC (see Figure S1).²⁴ For comparison, the large slope values ($\alpha \approx 4.3$ for PZT, and $\alpha \approx 5.4$ for BTO) indicate that another conduction mechanism exists in the pure ferroelectric films.²⁵ Therefore, it is reasonable to consider that the BTO/PZT interfaces in the superlattices mainly play a major role for the leakage current characteristic. Figure 5c is a schematic diagram showing the large space charges accumulated at the BTO/PZT interfaces and the movement of the space charges under an applied electric field. The intrinsic charged defects (such as oxygen vacancies and lead vacancies), which can be generated in ferroelectric films during the synthesis process, have a great effect on the leakage current due to their preference to accumulate at the BTO/PZT interfaces. To demonstrate the defects localized at the BTO/PZT interface, we have performed the X-ray photoelectron spectroscopy experiments by varying the probing depth (not shown here). The results show that Ti^{3+} ions exist at the BTO/PZT interfaces, indicating the high-density oxygen vacancies exist at BTO/PZT interfaces.²⁶ It has been reported that the heterointerfaces will attract and gather the oxygen vacancies because of the structural discontinuity.^{27,28} In addition, the charge re-distribution at the interfaces for the ferroelectric superlattices can be driven by the internal electric field formed in the constituent layer.^{17,29} On the other hand, the charges injecting from the electrodes may be scattered by the sharp BTO/PZT interfaces and the carrier mobility in the ferroelectric superlattices will be decreased.^{30,31} As mentioned above, the leakage current in the BTO/PZT superlattices decrease with the increase of the modulation periods. Therefore, the space charges distribution and the restricted movement by artificial interfaces largely reduce the leakage current in the BTO/PZT superlattices. The homogeneous distribution of defects can also influence the ferroelectric and dielectric properties of the BTO/PZT superlattices, which will be discussed in the following.

Figure 6 shows the P – E hysteresis loops of the BTO/PZT superlattices and the pure PZT and BTO thin films measured at 1 kHz and room temperature. The saturation polarizations (P_s) of the pure PZT and BTO thin films are about 66 and 21 $\mu\text{C}/\text{cm}^2$, respectively, which are comparable with those reported by the most previous works on the high-quality epitaxial films.^{20,32} The values of remanent polarization (P_r), P_s , and coercive field (E_c) values of the BTO/PZT superlattices are about 41 $\mu\text{C}/\text{cm}^2$, 17.1 $\mu\text{C}/\text{cm}^2$, and 230 kV/cm, respectively. The value of P_r is smaller than that of the PZT film ($P_r \approx 47 \mu\text{C}/\text{cm}^2$) but is larger than that of the BTO film ($P_r \approx 13 \mu\text{C}/\text{cm}^2$). It should be noted that the P_r value is larger than those reported in the

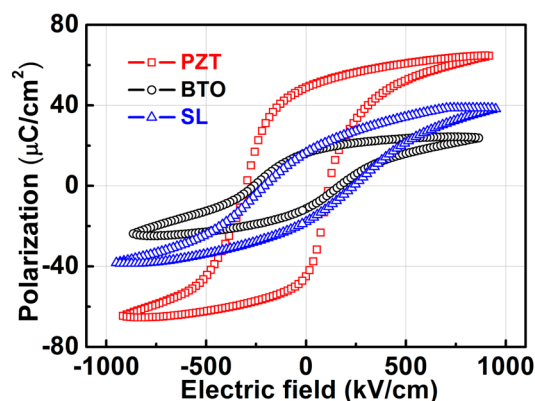


Figure 6. Polarization versus electric field (P – E) hysteresis loops for the pure PZT and BTO films, and the BTO/PZT superlattices at room temperature.

BTO-based¹² and PZT-based^{14,33} superlattices, which may be due to the high polarization of the two parent materials and the well-formed microstructure. Moreover, there are two important characteristics in the BTO/PZT superlattices. First, there is a relationship about the P_s for these three samples: $P_s^{\text{SL}} \approx (P_s^{\text{P}} + P_s^{\text{B}})/2$, where P_s^{SL} , P_s^{P} , and P_s^{B} are the P_s of the BTO/PZT superlattices, the pure PZT, and BTO films, respectively. Second, there is a great difference in the imprint among these three samples. The magnitude of the imprint can be defined as³⁴ $\Delta E = |E_+ - E_-|$, where E_+ and E_- present the positive and negative electric fields when the polarization is zero, respectively. For the pure PZT and BTO films, the values of ΔE are 185 and 92 kV/cm. In contrast, the P – E loop of the BTO/PZT superlattices became more symmetric and the ΔE decreased to 30 kV/cm. The above two characteristics of the BTO/PZT superlattices may also originate from the BTO/PZT interface effect. In the BTO/PZT superlattices, there is a large mismatch of ferroelectric polarization at the BTO/PZT interfaces, which caused large internal fields.^{17,35} The internal electric fields can further reduce the ferroelectric polarization in the BTO/PZT superlattices.³⁶ As we discussed earlier, the defect charges mainly accumulate at the BTO/PZT interfaces. The localized defects will compensate the bound charges, which is beneficial to reduce the depolarization field and keep the above relationship about P_s .^{18,37} Additionally, a 180° domain structure may form to reduce the depolarization field. Previous theoretical and experimental works have reported that the 180° domains in ferroelectric superlattices will arise naturally to weaken the strength of the electrostatic interactions between different ferroelectric layers and preserve their polar state.^{36,38} The imprint behavior in the BTO/PZT superlattices is also explained by the effect of BTO/PZT interfaces. In addition to the asymmetric electrode, many works have reported that the distribution of charged defects was responsible for the imprint of ferroelectric films.^{39,40} Compared to the pure PZT or BTO films, the homogeneously distributed charged defects in the BTO/PZT superlattices, which avoid the defects aggregation at the ferroelectric/electrode interfaces, lead to the relatively symmetrical hysteresis loops. Therefore, the artificial BTO/PZT interfaces in the BTO/PZT superlattices are beneficial for reducing the imprint.

We also studied the dielectric properties of the BTO/PZT superlattices from the perspective of the effect of BTO/PZT interfaces. Figure 7a shows the dielectric constant (ϵ_r) and loss ($\tan \delta$) as a function of the frequency for the BTO/PZT

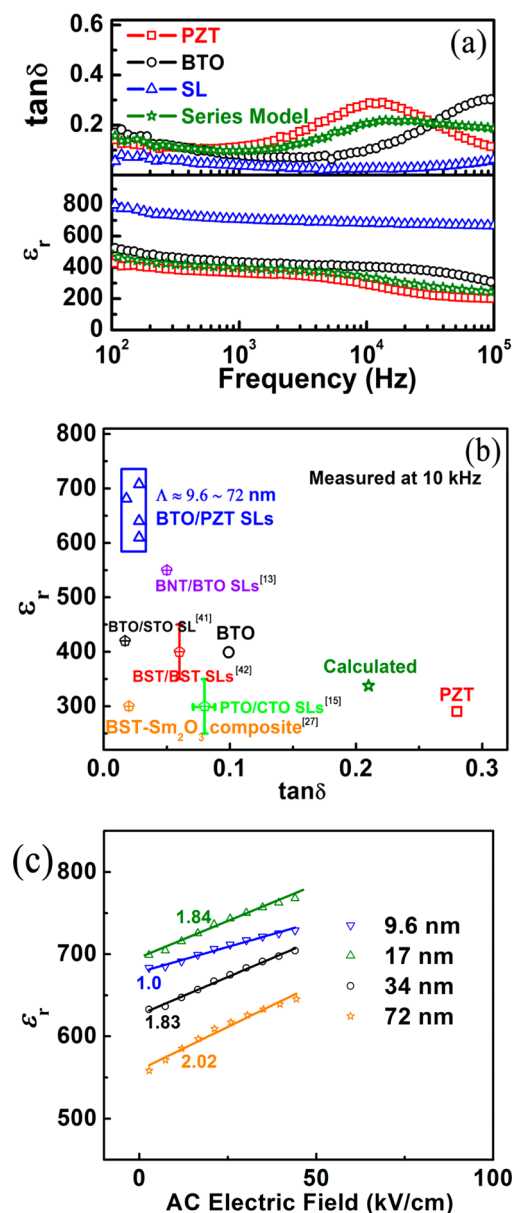


Figure 7. (a) Frequency dependence of the dielectric constants (ϵ_r) and loss tangent ($\tan \delta$) for the pure PZT and BTO films and the BTO/PZT superlattices. (b) ϵ_r versus $\tan \delta$ for the PZT and BTO films, and BTO/PZT superlattices with different modulation periods (9.6–72 nm) measured at 10 kHz. Some data for epitaxial ferroelectric superlattices and composite films from the literatures are also shown. (c) Dielectric constants as a function of AC electric field for BTO/PZT ferroelectric superlattices.

superlattices and the pure PZT and BTO films measured at room temperature. Compared with the BTO and PZT films, the BTO/PZT superlattices show a weak frequency dependence of ϵ_r and $\tan \delta$ in the range from 100 Hz to 100 kHz. The lower dielectric loss in the BTO/PZT superlattices is consistent with their lower leakage current, which is due to the lower concentration of the mobile charged defects restricted by the BTO/PZT interfaces. If we assume that the BTO/PZT superlattices are a series connection of the BTO and PZT layers, its effective dielectric constant (ϵ_{cal}) and loss ($\tan \delta_{\text{cal}}$) can be expressed as⁴

$$\epsilon_{\text{cal}} = \frac{t_{\text{BTO}} + t_{\text{PZT}}}{t_{\text{BTO}}/\epsilon_{\text{BTO}} + t_{\text{PZT}}/\epsilon_{\text{PZT}}} \quad (3)$$

$$\tan \delta_{\text{cal}} = \frac{t_{\text{PZT}}\epsilon_{\text{BTO}} \tan \delta_{\text{PZT}} + t_{\text{BTO}}\epsilon_{\text{PZT}} \tan \delta_{\text{BTO}}}{t_{\text{PZT}}\epsilon_{\text{BTO}} + t_{\text{BTO}}\epsilon_{\text{PZT}}} \quad (4)$$

where t_{BTO} and ϵ_{BTO} are the thickness and relative dielectric constant of the BTO layer and t_{PZT} and ϵ_{PZT} are the thickness and relative dielectric constant of the PZT layer. The calculated dielectric constant and loss are also shown in Figure 7a. The ϵ_r and $\tan \delta$ at 10 kHz for the BTO/PZT superlattices are calculated by using the series model to be approximately 336 and 0.21, respectively. In contrast, the measured values of ϵ_r and $\tan \delta$ for the BTO/PZT superlattices are 684 and 0.02, respectively (Figure 7b). Compared to the uncoupled condition, the BTO/PZT superlattices exhibit an enhancement of almost 100% in the dielectric constant. This means that the BTO/PZT interfaces play a very important role in the dielectric properties of the BTO/PZT superlattices. From Figure 7b, it can be seen that the BTO/PZT superlattices have high dielectric constants and very low dielectric loss as well, compared with other ferroelectric superlattices and composite films.^{13,15,27,41,42} In those previous works, the enhanced dielectric constants were mainly considered for the strain effect and Maxwell–Wagner effect. However, in this study, the mechanism for the enhanced dielectric properties may be different from those reported. On one hand, in the BTO/PZT superlattices, the PZT and BTO have the same crystalline structure with a very similar lattice constant. The lattice mismatch between them is very small ($\sim 1.0\%$), much less than that between the BaTiO₃ and SrTiO₃ in the BaTiO₃/SrTiO₃ superlattices ($\sim 2.3\%$).^{12,19} Therefore, it can be considered that the strain effects induced by the lattice mismatch between the PZT and BTO layers is not a major factor. On the other hand, if the Maxwell–Wagner effect plays an important role in the dielectric properties, the value of dielectric loss will increase with the dielectric constants.^{42,43} We measured the dielectric properties of the BTO/PZT superlattices with different modulation periods (Figure S2), and the results show that the dielectric constant increases with the increase of the modulation period. However, as shown in Figure 7b, the dielectric loss measured at 10 kHz for the BTO/PZT superlattices with different modulations (from 9.6 to 72 nm) is as low as 0.02–0.03 and did not change significantly with the increase of the dielectric constant. Therefore, it is possible to exclude the role of Maxwell–Wagner effect in our BTO/PZT superlattice.^{13,43} Figure 7c shows dielectric constants as a function of subcoercive AC electric field for the BTO/PZT superlattices with different modulation periods at 10 kHz. The curve slopes decrease with the increase of the modulation periods. Khan et al. have reported that the smaller value of slope, the less dominant are the effects of defects on the dielectric properties of the film.⁴⁶ The enhanced dielectric constant in the BTO/PZT superlattices is probably due to that the space charges accumulated at the BTO/PZT interfaces, which can reduce the pinning effect of defects on the motion of domain walls.^{44,45,47} Therefore, a low excitation field can easily makes the motion of domain walls, and the dependence of dielectric constant on the electric field is relatively weak. These above results further confirm that the BTO/PZT interfaces play a very important role for the enhanced electrical properties of the BTO/PZT superlattices.

CONCLUSIONS

In this study, we successfully fabricated the high-quality BTO/PZT ferroelectric superlattices on the (001) SrTiO₃ substrates by PLD. Compared to the parent materials of BTO and PZT, the microstructure, leakage behavior, and ferroelectric and dielectric properties of the BTO/PZT superlattice have been systematically investigated. The superlattices showed a low leakage current and space charge limited current mechanism, which is mainly due to the confined defect charges that distributed at the BTO/PZT interfaces. The defect charges accumulated at the BTO/PZT interfaces can reduce a depolarizing field and decrease the imprint in the P - E hysteresis loops. Moreover, the dielectric properties can be improved strongly in the BTO/PZT superlattices compared with the pure PZT and BTO films. Based on these experimental results, it can be considered that the BTO/PZT interfaces play a very significant role for the enhanced electrical properties of the BTO/PZT superlattices.

ASSOCIATED CONTENT

Supporting Information

The Supporting Information is available free of charge on the ACS Publications website at DOI: 10.1021/acsami.5b12098.

J - E curves for (BTO _{Λ /2}/PZT _{Λ /2}) superlattices with different modulation periods (Λ), $\ln J$ vs $\ln E$ for the BTO/PZT superlattices with $\Lambda \sim 17$ nm at different temperatures, and ϵ_r and $\tan \delta$ vs frequency for superlattices with different Λ (PDF)

AUTHOR INFORMATION

Corresponding Author

*E-mail: wangzj@imr.ac.cn.

Notes

The authors declare no competing financial interest.

ACKNOWLEDGMENTS

We gratefully acknowledge the partial support of this work by the Hundred Talents Program of the Chinese Academy of Sciences, the National Natural Science Foundation of China (Grant No. 51172238).

REFERENCES

- (1) Scott, J. F. Applications of Modern Ferroelectrics. *Science* **2007**, *315*, 954–959.
- (2) Mathews, S.; Ramesh, R.; Venkatesan, T.; Benedetto, J. Ferroelectric Field Effect Transistor Based on Epitaxial Perovskite Heterostructures. *Science* **1997**, *276*, 238–240.
- (3) Dawber, M.; Rabe, K. M.; Scott, J. F. Physics of Thin-Film Ferroelectric Oxides. *Rev. Mod. Phys.* **2005**, *77*, 1083.
- (4) Tagantsev, A. K.; Sherman, V. O.; Astafiev, K. F.; Venkatesh, J.; Setter, N. Ferroelectric Materials for Microwave Tunable Applications. *J. Electroceram.* **2003**, *11*, 5–66.
- (5) Wang, Y.; Shao, Q. Y.; Liu, J. M. Enhanced Fatigue-Endurance of Ferroelectric Pb_{1-x}Sr_x(Zr_{0.52}Ti_{0.48})O₃ Thin Films Prepared by Sol-Gel Method. *Appl. Phys. Lett.* **2006**, *88*, 122902.
- (6) Wang, Z. J.; Cao, Z. P.; Otsuka, Y.; Yoshikawa, N.; Kokawa, H.; Taniguchi, S. Low-Temperature Growth of Ferroelectric Lead Zirconate Titanate Thin Films Using the Magnetic Field of Low Power 2.45 GHz Microwave Irradiation. *Appl. Phys. Lett.* **2008**, *92*, 222905.
- (7) Chen, F.; Liu, Q. Z.; Wang, H. F.; Zhang, F. H.; Wu, W. Polarization Switching and Fatigue in PbZr_{0.52}Ti_{0.48}O₃ Films Sandwiched by Oxide Electrodes with Different Carrier Types. *Appl. Phys. Lett.* **2007**, *90*, 192907.
- (8) Dawber, M.; Stucki, N.; Lichtensteiger, C.; Gariglio, S.; Ghosez, P.; Triscone, J. M. Tailoring the Properties of Artificially Layered Ferroelectric Superlattices. *Adv. Mater.* **2007**, *19*, 4153–4159.
- (9) Zubko, P.; Gariglio, S.; Gabay, M.; Ghosez, P.; Triscone, J.-M. Interface Physics in Complex Oxide Heterostructures. *Annu. Rev. Condens. Matter Phys.* **2011**, *2*, 141–165.
- (10) Saha-Dasgupta, T. Ferroic Properties in Bi-Component Perovskites: Artificial Superlattices and Naturally Forming Compounds. *J. Phys.: Condens. Matter* **2014**, *26*, 193201.
- (11) Tenne, D. A.; Bruchhausen, A.; Lanzillotti-Kimura, N. D.; Fainstein, A.; Katiyar, R. S.; Cantarero, A.; Soukiassian, A.; Vaithyanathan, V.; Haeni, J. H.; Tian, W.; Schlom, D. G.; Choi, K. J.; Kim, D. M.; Eom, C. B.; Sun, H. P.; Pan, X. Q.; Li, Y. L.; Chen, L. Q.; Jia, Q. X.; Nakhmanson, S. M.; Rabe, K. M.; Xi, X. X. Probing Nanoscale Ferroelectricity by Ultraviolet Raman Spectroscopy. *Science* **2006**, *313*, 1614–1616.
- (12) Lee, H. N.; Christen, H. M.; Chisholm, M. F.; Rouleau, C. M.; Lowndes, D. H. Strong Polarization Enhancement in Asymmetric Three-Component Ferroelectric Superlattices. *Nature* **2005**, *433*, 395–399.
- (13) Bousquet, M.; Batista, L.; Dellis, J. L.; Boule, A.; Rabe, U.; Durand-Drouhin, O.; Gagou, Y.; Dupont, L.; Viallet, V.; Zeinert, A.; Hirsekorn, S.; Lemée, N. Structural and Electrical Properties of Bi_{0.5}Na_{0.5}TiO₃ Based Superlattices Grown by Pulsed Laser Deposition. *J. Appl. Phys.* **2014**, *116*, 194104.
- (14) Boldyreva, K.; Pintilie, L.; Lotnyk, A.; Misirliglu, I. B.; Alexe, M.; Hesse, D. Thickness-Driven Antiferroelectric-to-Ferroelectric Phase Transition of Thin PbZrO₃ Layers in Epitaxial PbZrO₃/Pb(Zr_{0.8}Ti_{0.2})O₃ Multilayers. *Appl. Phys. Lett.* **2007**, *91*, 122915.
- (15) Sinsheimer, J.; Callori, S. J.; Bein, B.; Benkara, Y.; Daley, J.; Coraor, J.; Su, D.; Stephens, P. W.; Dawber, M. Engineering Polarization Rotation in a Ferroelectric Superlattice. *Phys. Rev. Lett.* **2012**, *109*, 167601.
- (16) Okatan, M.; Mantese, J.; Alpay, S. Polarization Coupling in Ferroelectric Multilayers. *Phys. Rev. B: Condens. Matter Mater. Phys.* **2009**, *79*, 174113.
- (17) Okatan, M. B.; Misirliglu, I. B.; Alpay, S. P. Contribution of Space Charges to the Polarization of Ferroelectric Superlattices and Its Effect on Dielectric Properties. *Phys. Rev. B: Condens. Matter Mater. Phys.* **2010**, *82*, 094115.
- (18) Dawber, M.; Bousquet, E. New Developments in Artificially Layered Ferroelectric Oxide Superlattices. *MRS Bull.* **2013**, *38*, 1048–1055.
- (19) Tabata, H.; Tanaka, H.; Kawai, T. Formation of Artificial BaTiO₃/SrTiO₃ Superlattices Using Pulsed Laser Deposition and their Dielectric Properties. *Appl. Phys. Lett.* **1994**, *65*, 1970.
- (20) Mukherjee, D.; Hordagoda, M.; Lampen, P.; Phan, M.-H.; Srikanth, H.; Witanachchi, S.; Mukherjee, P. Simultaneous Enhancements of Polarization and Magnetization in Epitaxial Pb(Zr_{0.52}Ti_{0.48})O₃/La_{0.7}Sr_{0.3}MnO₃ Multiferroic Heterostructures Enabled by Ultrathin CoFe₂O₄ Sandwich Layers. *Phys. Rev. B: Condens. Matter Mater. Phys.* **2015**, *91*, 054419.
- (21) Reitz, C.; Leufke, P. M.; Hahn, H.; Brezesinski, T. Ordered Mesoporous Thin Film Ferroelectrics of Biaxially Textured Lead Zirconate Titanate (PZT) by Chemical Solution Deposition. *Chem. Mater.* **2014**, *26*, 2195–2202.
- (22) Le Marrec, F.; Farhi, R.; El Marssi, M.; Dellis, J. L.; Karkut, M. G.; Ariosa, D. Ferroelectric PbTiO₃/BaTiO₃ Superlattices: Growth Anomalies and Confined Modes. *Phys. Rev. B: Condens. Matter Mater. Phys.* **2000**, *61*, R6447.
- (23) Liang, X.; Clarke, D. R. Relation between Thermoelectric Properties and Phase Equilibria in the ZnO–In₂O₃ Binary System. *Acta Mater.* **2014**, *63*, 191–201.
- (24) Li, W.; Zhao, R.; Tang, R.; Chen, A.; Zhang, W.; Lu, X.; Wang, H.; Yang, H. Vertical-Interface-Manipulated Conduction Behavior in Nanocomposite Oxide Thin Films. *ACS Appl. Mater. Interfaces* **2014**, *6*, 5356–5361.

- (25) Barman, R.; Kaur, D. Leakage Current Behavior of BiFeO₃/BiMnO₃ Multilayer Fabricated by Pulsed Laser Deposition. *J. Alloys Compd.* **2015**, *644*, 506–512.
- (26) Ootsuki, S.; Ikeno, H.; Umeda, Y.; Moriwake, H.; Kuwabara, A.; Kido, O.; Ueda, S.; Tanaka, I.; Fujikawa, Y.; Mizoguchi, T. Ab-Initio Multiplet Calculation of Oxygen Vacancy Effect on Ti-L_{2,3} Electron Energy Loss near Edge Structures of BaTiO₃. *Appl. Phys. Lett.* **2011**, *99*, 233109.
- (27) Lee, O.; Harrington, S. A.; Kursumovic, A.; Defay, E.; Wang, H.; Bi, Z.; Tsai, C. F.; Yan, L.; Jia, Q.; MacManus-Driscoll, J. L. Extremely High Tunability and Low Loss in Nanoscaffold Ferroelectric Films. *Nano Lett.* **2012**, *12*, 4311–4317.
- (28) Lee, S.; Sangle, A.; Lu, P.; Chen, A.; Zhang, W.; Lee, J. S.; Wang, H.; Jia, Q.; MacManus-Driscoll, J. L. Novel Electroforming-Free Nanoscaffold Memristor with Very High Uniformity, Tunability, and Density. *Adv. Mater.* **2014**, *26*, 6284–6289.
- (29) Lim, K. G.; Chew, K. H.; Wang, D. Y.; Ong, L. H.; Iwata, M. Charge Compensation Phenomena for Polarization Discontinuities in Ferroelectric Superlattices. *Europhys. Lett.* **2014**, *108*, 67011.
- (30) Pintilie, L. Advanced Electrical Characterization of Ferroelectric Thin Films: Facts and Artifacts. *J. Optoelectron. Adv. Mater.* **2009**, *11* (3), 215–228.
- (31) Zhao, R.; Li, W.; Chen, A.; Zhang, W.; Yang, J.; Liang, Y.; Tang, R.; Wang, H.; Yang, H. Manipulating Leakage Behavior via Distribution of Interfaces in Oxide Thin Films. *Appl. Phys. Lett.* **2014**, *105*, 072907.
- (32) Chen, A. P.; Khatkhatay, F.; Zhang, W.; Jacob, C.; Jiao, L.; Wang, H. Strong Oxygen Pressure Dependence of Ferroelectricity in BaTiO₃/SrRuO₃/SrTiO₃ Epitaxial Heterostructures. *J. Appl. Phys.* **2013**, *114*, 124101.
- (33) Dussan, S.; Kumar, A.; Scott, J. F.; Priya, S.; Katiyar, R. S. Room Temperature Multiferroic Effects in Superlattice Nanocapacitors. *Appl. Phys. Lett.* **2010**, *97*, 252902.
- (34) Grossmann, M.; Lohse, O.; Bolten, D.; Boettger, U.; Schneller, T.; Waser, R. The Interface Screening Model as Origin of Imprint in PbZr_xTi_{1-x}O₃ Thin Films. I. Dopant, Illumination, and Bias Dependence. *J. Appl. Phys.* **2002**, *92*, 2680.
- (35) Misirlioglu, I. B.; Kesim, M. T.; Alpay, S. P. Strong Dependence of Dielectric Properties on Electrical Boundary Conditions and Interfaces in Ferroelectric Superlattices. *Appl. Phys. Lett.* **2014**, *104*, 022906.
- (36) Zubko, P.; Jecklin, N.; Torres-Pardo, A.; Aguado-Puente, P.; Gloter, A.; Lichtensteiger, C.; Junquera, J.; Stephan, O.; Triscone, J. M. Electrostatic Coupling and Local Structural Distortions at Interfaces in Ferroelectric/Paraelectric Superlattices. *Nano Lett.* **2012**, *12*, 2846–2851.
- (37) Lu, X. Y.; Cao, W. W.; Li, H. Space Charge Effect in Ultrathin Ferroelectric Films. *J. Appl. Phys.* **2012**, *111*, 084103.
- (38) Stephanovich, V. A.; Luk'yanchuk, I. A.; Karkut, M. G. Domain-Enhanced Interlayer Coupling in Ferroelectric/Paraelectric Superlattices. *Phys. Rev. Lett.* **2005**, *94*, 047601.
- (39) Wang, X. L.; Li, B.; Zhong, X. L.; Zhang, Y.; Wang, J. B.; Zhou, Y. C. Effects of Space Charge Distribution on Ferroelectric Hysteresis Loops Considering the Inhomogeneous Built-in Electric Field: A Phase Field Simulation. *J. Appl. Phys.* **2012**, *112*, 114103.
- (40) Misirlioglu, I. B.; Okatan, M. B.; Alpay, S. P. Asymmetric Hysteresis Loops and Smearing of the Dielectric Anomaly at the Transition Temperature Due to Space Charges in Ferroelectric Thin Films. *J. Appl. Phys.* **2010**, *108*, 034105.
- (41) Tsai, H.-N.; Liang, Y.-C.; Lee, H.-Y. Characteristics of Sputter-Deposited BaTiO₃/SrTiO₃ Artificial Superlattice Films on an LaNiO₃-Coated SrTiO₃ Substrate. *J. Cryst. Growth* **2005**, *284*, 65–72.
- (42) O'Neill, D.; Bowman, R. M.; Gregg, J. M. Dielectric Enhancement and Maxwell-Wagner Effects in Ferroelectric Superlattice Structures. *Appl. Phys. Lett.* **2000**, *77*, 1520.
- (43) Corbett, M. H.; Bowman, R. M.; Gregg, J. M.; Foord, D. T. Enhancement of Dielectric Constant and Associated Coupling of Polarization Behavior in Thin Film Relaxor Superlattices. *Appl. Phys. Lett.* **2001**, *79*, 815.
- (44) Zubko, P.; Stucki, N.; Lichtensteiger, C.; Triscone, J. M. X-Ray Diffraction Studies of 180° Ferroelectric Domains in PbTiO₃/SrTiO₃ Superlattices under an Applied Electric Field. *Phys. Rev. Lett.* **2010**, *104*, 187601.
- (45) García, J. E.; Pérez, R.; Albareda, A. Contribution of Reversible Processes to the Non-Linear Dielectric Response in Hard Lead Zirconate Titanate Ceramics. *J. Phys.: Condens. Matter* **2005**, *17*, 7143–7150.
- (46) Khan, A. I.; Yu, P.; Trassin, M.; Lee, M. J.; You, L.; Salahuddin, S. The Effects of Strain Relaxation on the Dielectric Properties of Epitaxial Ferroelectric Pb(Zr_{0.2}Ti_{0.8})TiO₃ Thin Films. *Appl. Phys. Lett.* **2014**, *105*, 022903.
- (47) Xu, F.; Trolier-McKinstry, S.; Ren, W.; Xu, B.; Xie, Z. L.; Hemker, K. J. Domain Wall Motion and its Contribution to the Dielectric and Piezoelectric Properties of Lead Zirconate Titanate Films. *J. Appl. Phys.* **2001**, *89*, 1336.